5.1 THE MICROPHYSICS OF THE 14 JUNE 2011 NORMAN, OKLAHOMA, DOWNBURST FROM DUAL-POLARIZATION AND DUAL-DOPPLER RADAR MEASUREMENTS

Vivek N. Mahale*[1,2], Guifu Zhang[1,2] and Ming Xue[2,3]
[1]Advanced Radar Research Center, University of Oklahoma
[2] School of Meteorology, University of Oklahoma
[3]Center for Analysis and Prediction of Storms, University of Oklahoma

1. INTRODUCTION

Downbursts are areas of strong, damaging winds that are produced by convective downdrafts (AMS 2001). On radar velocity measurements, there must be a differential velocity (i.e. radial divergence signature) >10 m s^{-1} for a storm to be classified as a downburst. Downbursts have been classified by length and precipitation amount. Microbursts are <4 km in length and usually have winds that last 2 to 5 minutes. Macrobursts are >4 km in length, and are especially common in bow echoes. Dry downbursts have <0.01” rainfall at the surface, and wet downbursts have >0.01” rainfall. Wet downbursts may also have hail in addition to rain.

Downbursts were heavily studied in the 1970s and 1980s due to significant impacts on aviation (e.g., Fujita and Caracena 1977; NTSB 1983; Fujita 1985, 1986). In 1985, the crash of Delta Flight 191 at the Dallas-Fort Worth airport led the Federal Aviation Administration (FAA) to conduct a study on how dangerous, low-level wind shear could be detected (Whiton et al. 1998). The result was funding by Congress for the C-band Terminal Doppler Weather Radar (TDWR) program. This program is separate from the national Next-Generation Radar (NEXRAD; NEXRAD 1980), S-band radar network. The FAA chose the C-band frequency for the TDWR radars because of the need for a high maximum unambiguous velocity measurement; the FAA also didn’t require long-range information as needed from NEXRAD. Since the product of the maximum unambiguous range and maximum unambiguous velocity is constant (i.e. the Doppler dilemma), the shorter range from C-band allowed for greater maximum unambiguous velocity measurements through the use of a pulse repetition frequency (PRF) agility scheme (Whiton et al. 1998).

TDWR radars are currently not dual-polarized. In the spring of 2003, the National Severe Storms Laboratory (NSSL) Joint Polarization Experiment (JPOLE) project demonstrated improvements that dual polarization (dual-pol) radars provided for rainfall estimation, hydrometeor classification, and data quality (ROC 2013). As a result, the NEXRAD radars began upgrades to dual-pol in 2011; the dual-pol upgrade is expected to be completed in 2013. Dual-pol NEXRADs provide both conventional and dual-polarized data (Doviak and Zrnić, 1993; Zrnić and Ryzhkov 1999). The radar observables include: 1) Radar reflectivity factor (henceforth known as radar reflectivity, Z_H), which is the reflectivity factor for horizontal polarization; 2) Differential reflectivity (Z_{DR}), which is ten times the logarithmic ratio of the reflectivity factors at the horizontal and vertical polarizations; 3) Correlation coefficient (ρ_{hv}), which is the correlation coefficient between copolar horizontally and vertically polarized echo signals; 4) Differential phase (Φ_{DP}), which is the difference in phase between the horizontally and vertically polarized fields caused by backscattering; 5) Radial velocity, which is the component of velocity either inbound or outbound from the radar; and 6) Spectrum width, which is the standard deviation of the velocity spectrum. By using the additional data from dual-pol radars, a better understanding of the microphysical evolution of precipitation is possible. For example, this has already been an ongoing area of research for supercells (e.g., Kumjian and Ryzhkov 2008).

In this study, the microphysical evolution of a downburst is analyzed through the use of the dual-pol KOUN Weather Surveillance Radar (WSR-88D) located in Norman, Oklahoma. First, an overview of the downburst event is given. This is followed by RHIs of dual-pol observations in the beginning and latter stages of the downburst. Next, a hydrometeor classification algorithm is applied to the data. Finally, dual-Doppler wind analysis is assessed alongside the hydrometeor classification.

2. EVENT OVERVIEW

On 14 June 2011, a downburst affected Norman, Oklahoma, in the early evening between 7:25 to 7:40 pm CDT (0025 to 0040 UTC). The thunderstorm that caused the downburst was a

**Corresponding author address*: Vivek Mahale, School of Meteorology
120 David L. Boren, Suite #5900, Norman, OK 73072-7307, E-mail: vmahale@ou.edu

right-mover that split off initial convection which initiated ahead of a weak surface cold front (Fig. 1). The thermodynamics of the atmosphere were highly conducive for storms to produce downbursts in Central Oklahoma on that day (Fig. 2).

2.1 ***Surface Observations***

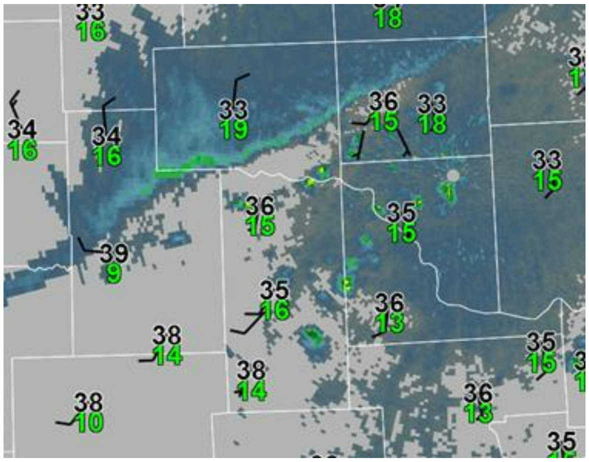

Fig. 1. KTLX radar reflectivity, surface wind barbs (full barb ≡ 5 m s^{-1}; half barb ≡ 2.5 m s^{-1}),surface temperature and dew point at 2315 UTC.

Surface winds in excess of 35 m s^{-1} (>80 mph) and hail in excess of 4 cm diameter were reported from the storm (NWS Norman 2013). Widespread wind damage occurred across Norman (Fig. 3), including at Max Westheimer Airport (Fig 4). The area of damage was over 4 km in length; therefore, the downburst can be classified a macroburst by size.

The Norman Mesonet located near the airport, had a measured sustained wind speed of 20 m s^{-1} and a 5 hPa pressure rise (Fig. 5). The site also received 28 mm of rainfall within 20 minutes, which is equivalent to a rainfall rate over 80 mm hr^{-1}. Therefore, the storm is classified as a wet downburst by precipitation.

2.1 ***Mesoscale Environment***

On the mesoscale scale, a cold front was located across central Oklahoma (Fig. 2). The temperature gradient along the cold front was weak (~3 to 4°C). The wind shift along the cold front was nearly 180 degrees; thus, surface convergence was present along the boundary. The convergence along the cold front was also detected by the KTLX WSR-88D. A weak line of reflectivity indicated a buildup particulates and insects along the area of convergence. The thunderstorm that would produce the downburst, initiated just ahead of a cold front just before 2315 UTC on 14 June 2011.

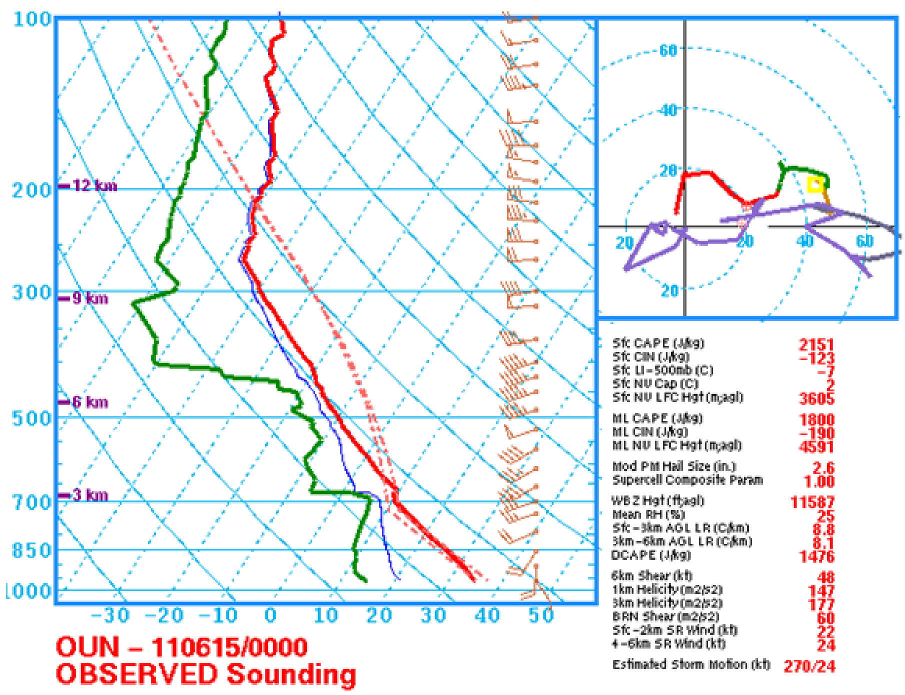

Fig. 2. KOUN sounding at 0000 UTC on 15 June 2011 (courtesy SPC).

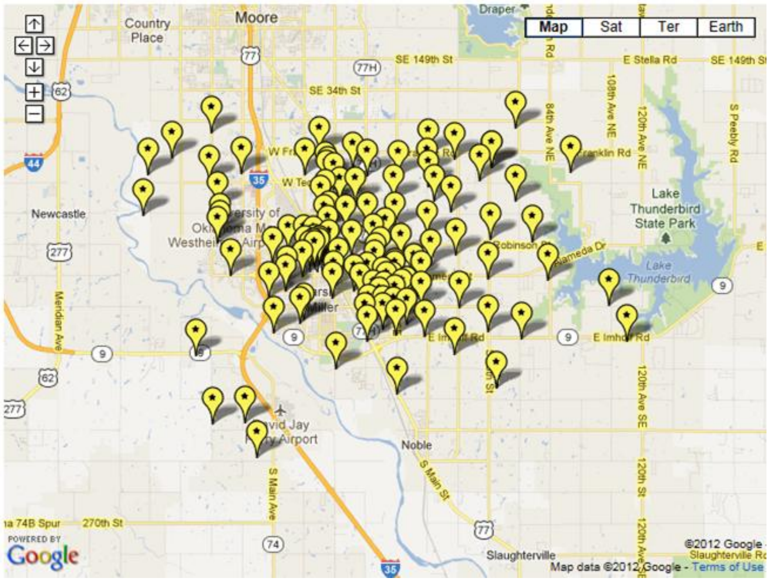

Fig. 3. Map of wind damage reports (courtesy NWS Norman).

Fig. 4. Photo of the downburst and damage at Max Westheimer Airport (courtesy Robin Tanamachi).

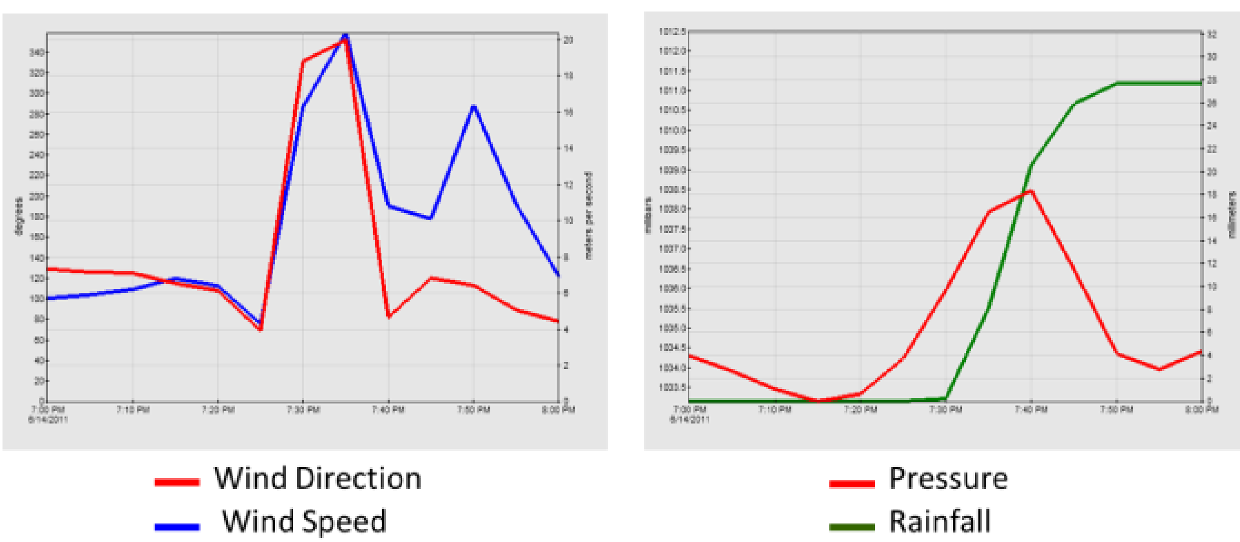

Fig. 5. Norman Mesonet surface observations from the downburst.

The Norman (KOUN) sounding at 0000 UTC on 15 June 2011 was the closest spatial and temporal sounding to the downburst (Fig. 2). The downburst affected Norman just after 0020 UTC; therefore, the sounding should be a reasonable representation of the pre-storm environment. The atmosphere was moderately unstable as indicated by surface based convective available potential energy (SBCAPE) at ~2150 J kg^{-1}.

The atmosphere was also conducive for downbursts. Large dew point depressions were present in the lowest 3 km; the dry layer in the lower atmosphere allows for evaporative cooling to strengthen the downdraft. Also, a nearly dry adiabatic (well-mixed) layer existed below the cloud layer, which is favorable for both dry and wet downbursts (Srivastava 1987). The downdraft CAPE (DCAPE) was ~1500 J kg^{-1}. DCAPE is defined as the maximum increase in kinetic energy (per unit mass) that could result from evaporative from some height to the surface (Emanuel 1994).

3. DUAL-POL OBSERVATIONS

Dual-pol observations of the storm were analyzed between the early stages of development through the time of the downburst. RHIs were constructed through the core to deduce the evolution of the storm. Interesting features are noted after the data were quality controlled.

3.1 *Quality Control*

Quality control was done on the radar data for this event. First, data where the horizontal or vertical signal-to-noise ratio (SNR) were less than 5 dB were removed. Noise was estimated by averaging radials on the extreme peripherally of precipitation and then accounting for range. This allowed for the calculation of SNR and the removal of the data. Second, using the horizontal and vertical SNR calculations, ρ_{hv} was corrected to account for SNR. Both of these quality control methods were implemented during the JPOLE experiment (Schuur et al. 2003).

3.2 *Dual-Pol Features*

In the developing stage of the storm, a well-

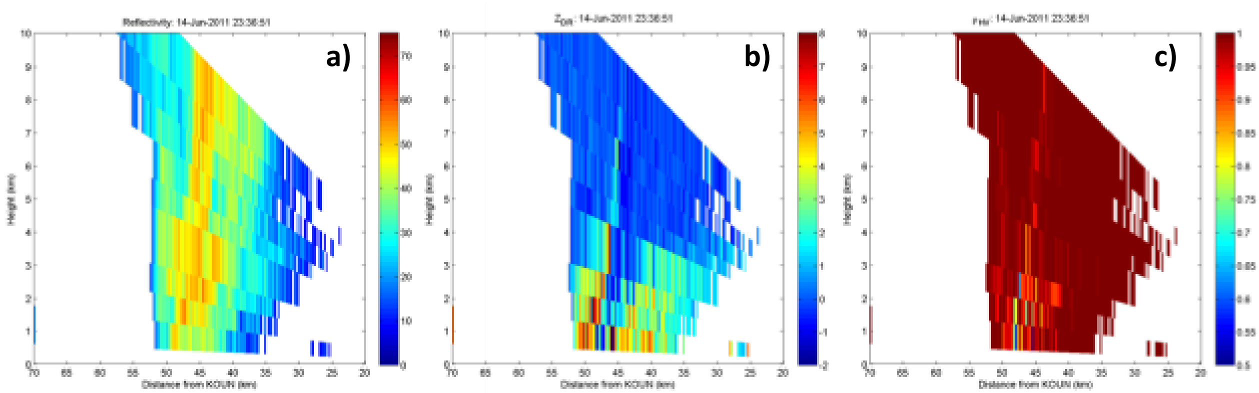

Fig. 6. RHI of (a) Z_H, (b) Z_{DR} and (c) ρ_{hv} at 2236 UTC. Note the presence of a Z_{DR} column and a low ρ_{hv} column.

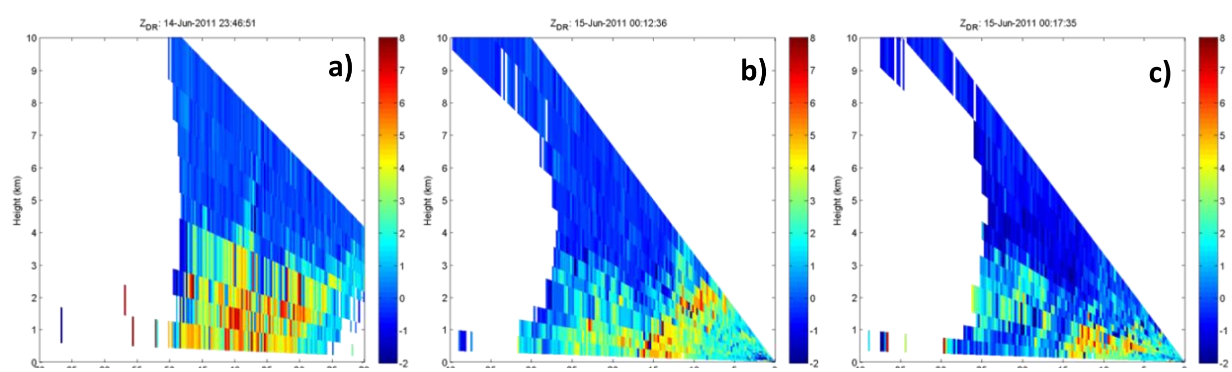

Fig. 7. RHI of Z_{DR} at (a) 2346, (b) 0012 and (c) 0017 UTC. Note the dissipation of the Z_{DR} by 0012 UTC, followed by a descending Z_{DR} minimum.

defined Z_{DR} column was present in the storm (Fig. 6b). This Z_{DR} column existed well-above the melting layer of ~4.5 km. Kumjian et al. (2012) found that Z_{DR} columns that penetrate above the freezing level indicate a very strong updraft. In this particular case, the Z_{DR} column extended to at least 7 km, or 2.5 km above the freezing level. There was also a low ρ_{hv} column co-located with the Z_{DR} column (Fig. 6c), suggesting mixed hydrometeors were present.

Even 10 minutes later at 2346 UTC, a Z_{DR} column was still present, suggesting that the updraft was still very intense (Fig. 7a). A strong updraft above the freezing level increases the potential for large hail growth. By 0012 UTC, the Z_{DR} column had dissipated (Fig. 7b). Instead, there was a descending minimum of Z_{DR} associated with the downburst (Fig. 7b and 7c). This feature had been seen previously by Wakimoto and Bringi (1988).

By 0027 UTC, a three-body scatter spike (TBSS) was present. A TBSS is a radar artifact that is caused by Mie scattering from a region of large hydrometeors—usually large, wet hail (Zrnić 1987).

When looking at ρ_{hv}, it is confirmed that this spike of reflectivity (Fig. 8a) on the backside of the storm was not associated with precipitation. The extremely low ρ_{hv} (<0.5) indicates non-meteorological targets (Fig. 8b).

The detection of these features is beneficial because Lemon (1998) found TBSS can often be a precursor of at least 2.5 cm diameter hail at the surface within 10 to 30 min.

4. HCA CLASSIFCATION

Due to hail contamination, drop size distribution (DSD) calculations cannot be done for this event. Therefore, another method to gain further understanding of the microphysical evolution of the storm is through the use of hydrometeor classification algorithm (HCA).

4.1 *Overview of HCA*

HCA algorithms were first studied by Straka and Zrnić (1993) and have become increasingly sophisticated over time (e.g., Zrnić and Ryzhkov 1999; Vivekanandan et al. 1999). More recently, Park et al. (2009) wrote paper describing the most recent version of the HCA for polarimetric WSR-88D radars. This HCA discriminates between 10 classes of radar echo: 1) ground clutter and anomalous propagation (GC/AP); 2) biological scatterers (BS); 3) dry aggregated snow (DS); 4) wet snow (WS); 5) crystals (CR); 6) graupel (GR); 7) 'bigdrops' (BD); 8) light and moderate rain (RA); 9)heavy rain (HR); and 10) a mixture of rain and hail (RH).

In this study, a simplified version of this Park et al. (2009) algorithm was utilized. The simplifications were: 1) No use of K_{DP}; 2) No attenuation correction for Z or Z_{DR}; 3) No confidence vectors; and 4) No hard thresholds.

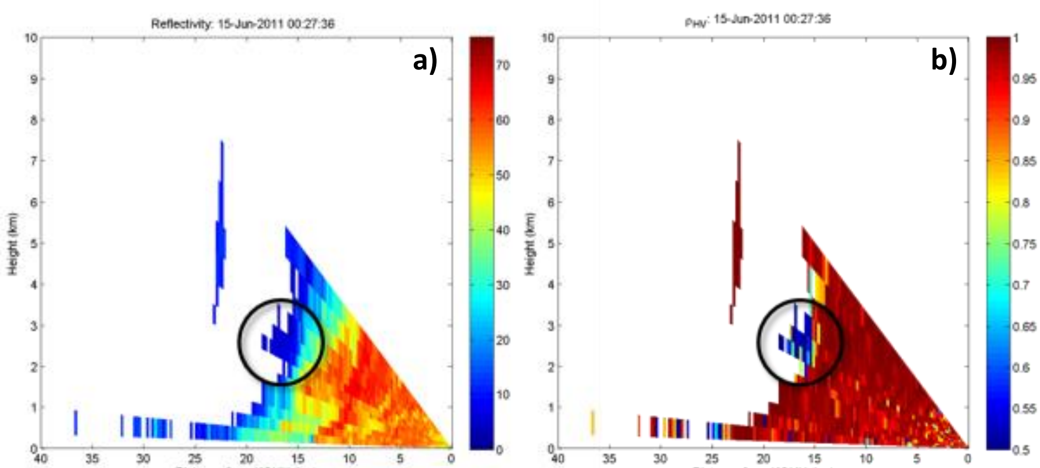

Fig. 8. RHI of (a) Z_H and (b) ρ_{hv} at 0027 UTC. Three-body scatter spike circled in black

Therefore, five variables were utilized for discrimination of hydrometer type: 1) horizontal radar reflectivity (Z_H); 2) differential reflectivity (Z_{DR}); 3) correlation coefficient (ρ_{hv}); 4) a texture parameter, SD(Z); and 5) another texture parameter, SD(Φ_{DP}). The texture fields were calculated for each gate by calculating the standard deviation along the radial using five gates (i.e. the two previous gates, the next two gates and the current gate along the radial were used for the calculation). More information can be found in Park et al. (2009) on this HCA method.

4.2 *HCA Storm Evolution*

In the early stages of the convective storm (as it was splitting), an area of graupel and hail/rain mix expanded significantly above the freezing level (~4.5 km). The greatest growth of this area of graupel and rain/hail mix occurred between 2336 and 2341 UTC (Fig. 9d and Fig. 10a). Initially, the majority of this growth was graupel. As noted previously, a deep Z_{DR} column suggested the presence of an intense updraft within the storm at 2336 UTC. Thus, the greatest expansion of graupel aloft occurred in the volume scan immediately after the updraft had increased in intensity.

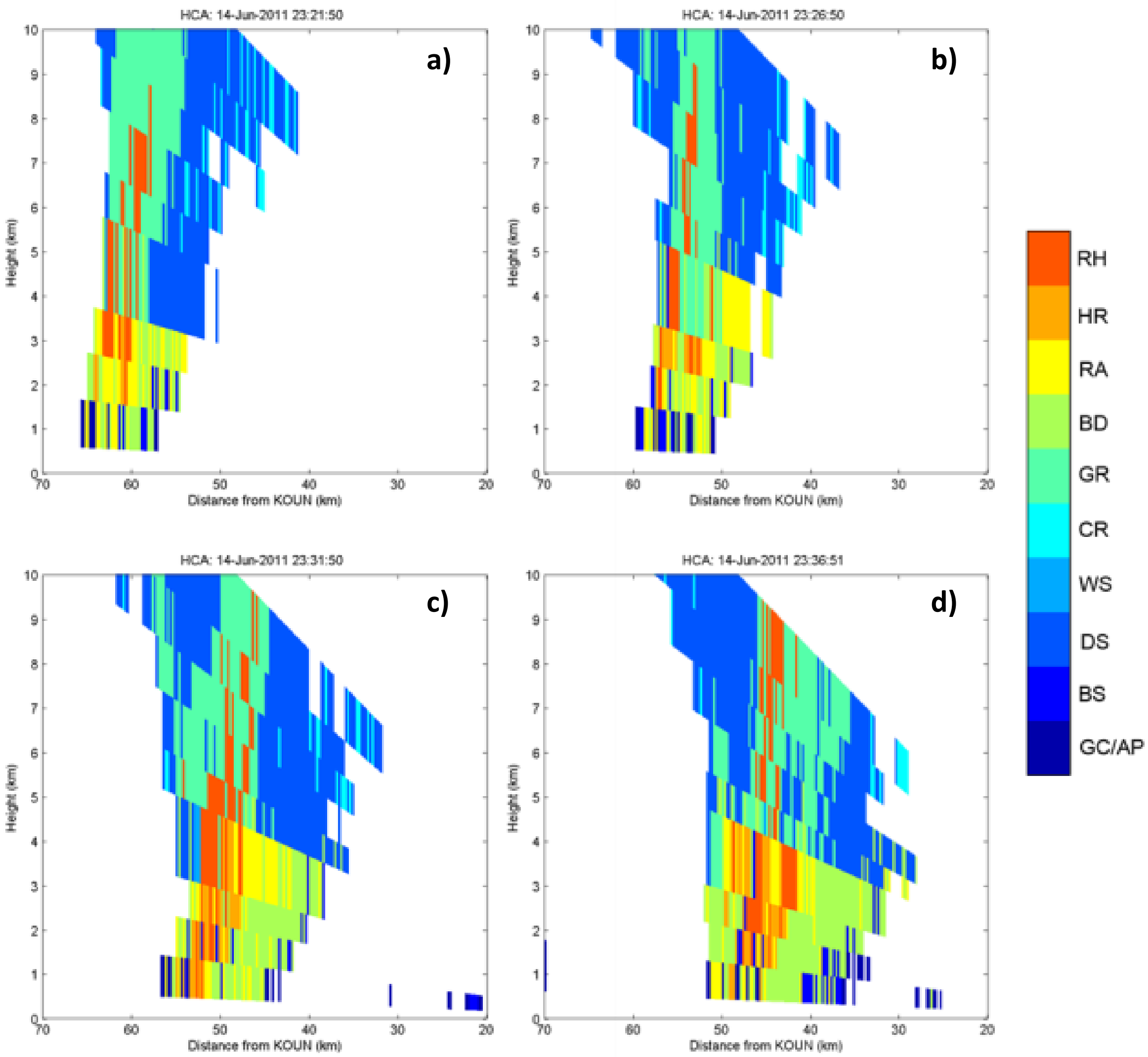

Fig. 9. RHI of HCA at (a) 2321, (b) 2326, (c) 2331, and (d) 2336 UTC.

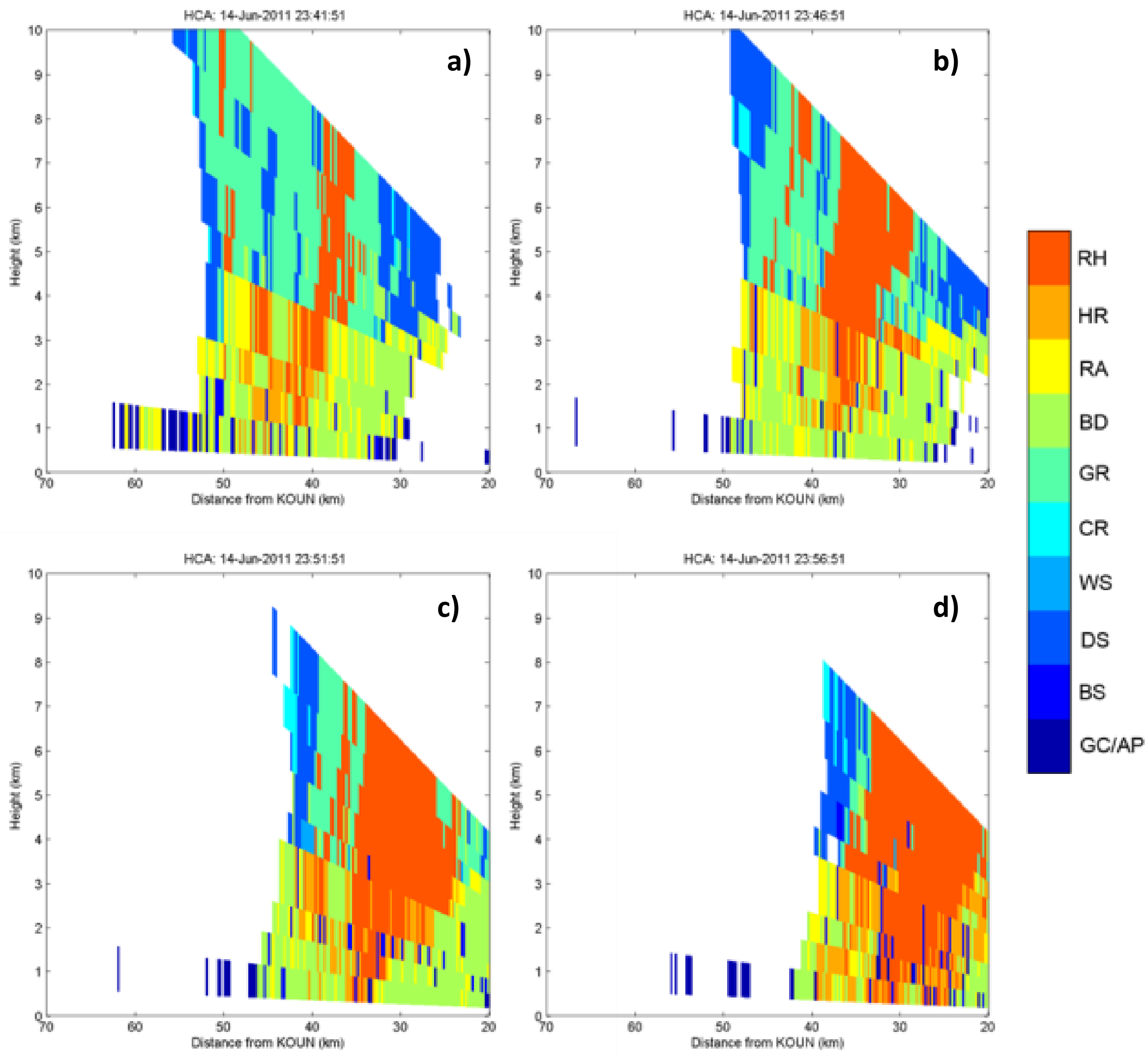

Fig. 10. RHI of HCA at (a) 2341, (b) 2346, (c) 2351, and (d) 2356 UTC.

Eventually the majority of the graupel evolved into a mixture of mostly rain and hail between 2341 and 2351 UTC (Fig. 10a-c). As mentioned previously, a Z_{DR} column was still present at this time, so it is expected that hail growth could occur due to a strong updraft. Also noted earlier, the atmosphere was highly conducive for downbursts on this day. Studies have shown that ice hydrometeors (i.e. hail) can play a significant role in downbursts by increasing the intensity of the downdraft compared to just rain (e.g., Srivastava 1987; Atkins and Wakimoto 1991). Therefore, it could be surmised that the rapid growth of an expansive rain and hail mixture would significantly increase the risk of a downburst on a day with similar thermodynamic conditions. Note that this was still ~30 min before the downburst caused damage at the surface.

After continued areal expansion, the area of rain and hail mixture eventually descended to the ground between 0012 and 0027 UTC (Fig. 11).

4.4 *Dual-Doppler Wind Analysis*

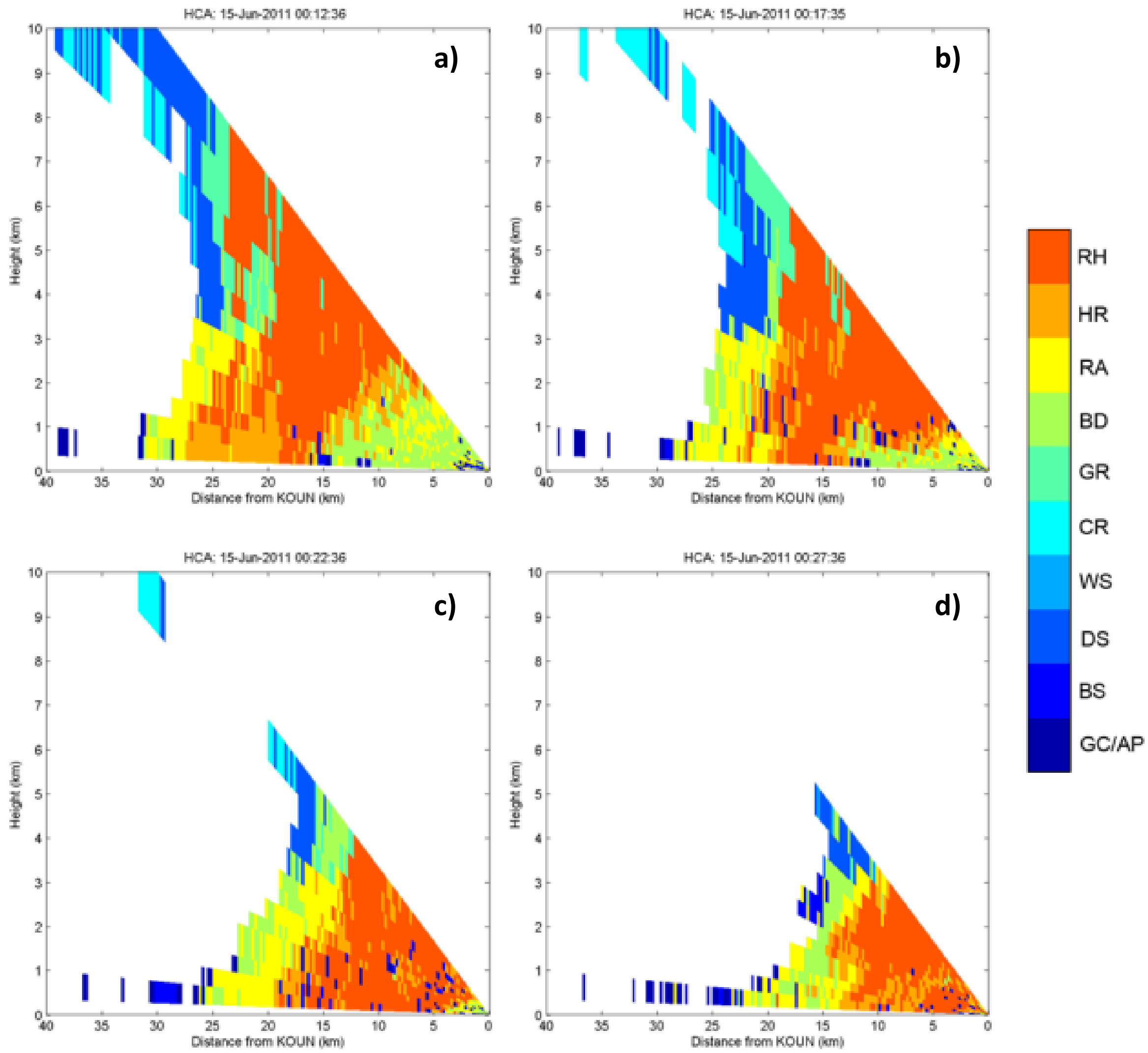

Fig. 11. RHI of HCA at (a) 0012, (b) 0017, (c) 0022, and (d) 0027 UTC.

Dual-Doppler analysis was conducted on the radar data using both KOUN and KTLX WSR-88Ds; however, due to the beam crossing angle, only one volume scan could be analyzed. The radar data were transformed from the radar coordinate system into a Cartesian coordinate system using National Center for Atmospheric Research's (NCAR) objective analysis software package REORDER (NCAR 1995). Once the objective analysis was complete, dual-Doppler analysis was done using NCAR's software package CEDRIC, which conducts its dual-Doppler analysis by finding the projection of the particle motion along the Doppler radar radial direction (NCAR 1998).

The 1 km dual-Doppler analysis at 0023 UTC indicated a divergent wind pattern, which is expected near the surface in a downburst (Fig. 12). In addition, there was very strong downward motion (~-20 m s^{-1}) at 1 km. Much of the downward motion in the dual-Doppler analysis was co-located in the rain and hail mixture, which is further confirmation of the wet downburst by radar observations.

5. SUMMARY

A thunderstorm that initiated ahead of a cold front split off and produced a significant downburst approximately within an hour time scale. Dual-pol observations indicated the presence of a strong

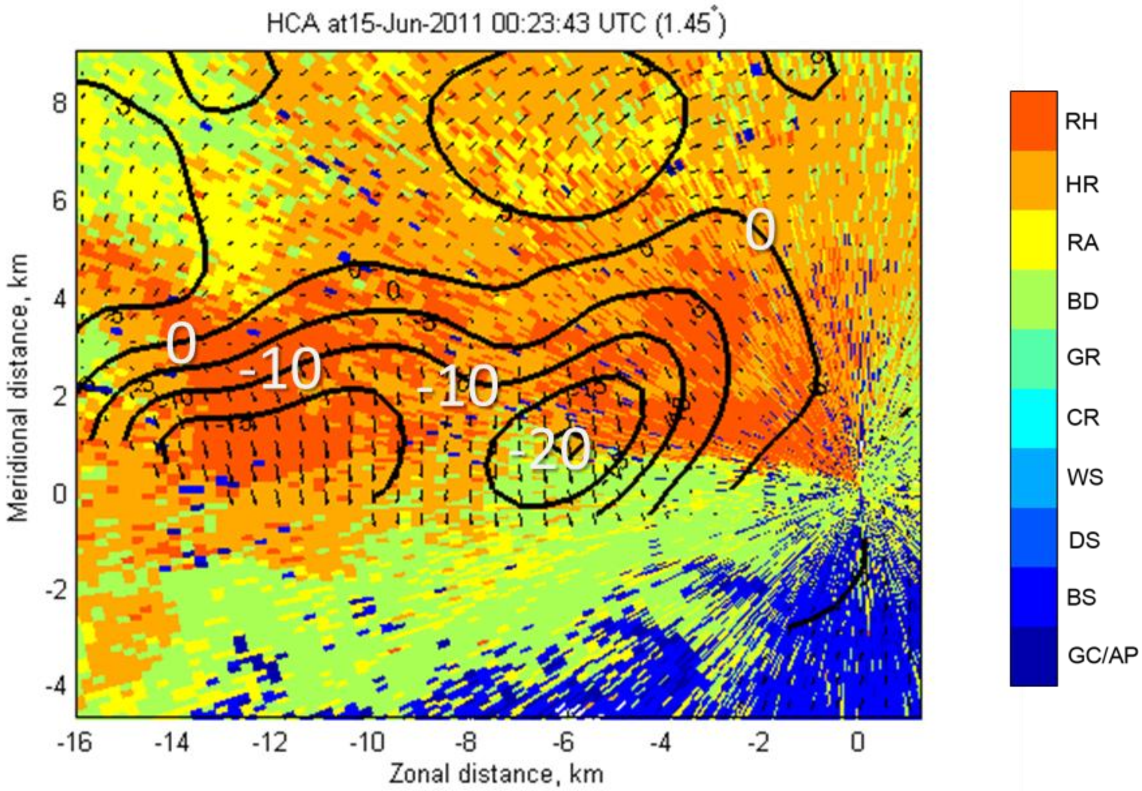

Fig. 12. 1.45° PPI HCA at 0023 UTC with 1 km dual-Doppler horizontal wind vectors and vertical motion (black contours).

updraft, well-above the freezing level. During this early stage, an area of mostly graupel and some rain/hail mix expanded aloft. Eventually, the graupel transitioned to nearly all hail and rain mixture above the freezing level. Eventually, this large area of hail and rain mixture descended to the ground during the downburst. This was verified using dual-Doppler analysis in conjunction with hydrometeor classification.

This study shows the advantages of dual-pol radars in microphysical studies. Without the added benefit of dual-pol observations, it is difficult to classify different hydrometeors or deduce updraft strength. However, through the use of HCA, the evolution of the microphysics within the storm is clearer though the aggregation of the different radar variables to derive the different classes. This demonstrates that dual-pol will allow the potential to further understand the microphysics and issue advanced warnings for hazardous weather.

ACKNOWLEDGMENTS

This work is supported by the National Science Foundation under NSF award 1046171.

REFERENCES

AMS, cited 2013: Glossary of Meteorology. [Available online at http://amsglossary.allenpress.com/glossary].

Atkins, N. T., and R. M. Wakimoto, 1991: Wet microburst activity over the southeastern United States: Implications for forecasting. *Wea. Forecasting*, **6,** 470–482.

Doviak, R., D. Zrnić, 1993: *Doppler Radar and Weather Observations*. Dover Publications, Inc, 562 pp.

Emanuel, K. A., 1994: *Atmospheric Convection.* Oxford University Press, 883 pp.

Fujita, T.T., 1985: Thw downburst. SMRP Res. Paper No. 210, NTIS PB-85-148880, 122 pp.

Fujita, T.T., 1986: DFW microburst. SMRP Res Paper No. 217, NTIS PB- 86-131638, 154 pp.

Fujita, T.T., and F. Caracena, 1977: An analysis of three weather-related aircraft accidents. *Bull. Amer. Meteor. Soc.,* **58,** 1164–1181.

Kumjian, M. R., and A. V. Ryzhkov, 2008: Polarimetric signatures in supercell thunderstorms. *J. Appl. Meteor. Climatol.*, **47,** 1940–1961.

Kumjian, M.R., S. M. Ganson, and A. V. Ryzhkov, 2012: Freezing of raindrops in deep convective updrafts: a microphysical and polarimetric model. *J. Atmos. Sci*., **69,** 3471–3490.

Lemon, L. R., 1998: The radar ''Three-body scatter spike'': An operational large-hail signature. *Wea. Forecasting*, **13,** 327–340.

National Center for Atmospheric Research, 1995: REORDER Installation and Use Manual for the Unix Version.

National Center for Atmospheric Research, 1998: CEDRIC: Custom Editing and Display of Reduced Information in Cartesian Space. decreases.

National Transportation Safety Board, 1983: Aircraft accident report: Pan American World Airways, Inc., Clipper 759, Boeing 727-235, N4737, New Orleans International Airport, Kenner, Louisiana, July 9, 1982. 113 pp. [NTIS PB 83-910402.]

National Weather Service Norman Forecast Office, cited 2013: The June 14, 2011 Severe Wind Event in Central Oklahoma. [Available online at http://www.srh.noaa.gov/oun/?n=events-20110614].

Next Generation Weather Radar (NEXRAD), 1980: Joint Program Development Plan, NEXRAD Joint System Program Office, Silver Spring, Maryland, 102 pp.

Radar Operations Center (ROC), cited 2012: Dual Polarization. [Available online at http://www.roc.noaa.gov/WSR88D/DualPol/Default.aspx].

Park, H. S., A. V. Ryzhkov, D. S. Zrnić, and K.-E. Kim, 2009: The hydrometeor classification algorithm for the polarimetric WSR-88D: Description and application to an MCS. *Wea. Forecasting*, **24,** 730–748.

Schuur, T. J., A. V. Ryzhkov, and P. L. Heinselman, 2003: Observations and classification of echoes with the polarimetric WSR-88D radar. NOAA/National Severe Storms Laboratory Rep., 46 pp.

Srivastava, R. C., 1987: A model of intense downdrafts driven by the melting and evaporation of precipitation. *J. Atmos. Sci*., **44,** 1752–1773.

Straka, J. M., and D. S. Zrnić, 1993: An algorithm to deduce hydrometeor types and contents from multiparameter radar data. Preprints, *26th Conf. on Radar Meteorology*, Norman, OK, Amer. Meteor. Soc., 513–516.

Vivekanandan, J., D. S. Zrnić, S. Ellis, D. Oye, A. V. Ryzhkov, and J. M. Straka, 1999: Cloud microphysics retrieval using S-band dual-polarization radar measurements. *Bull. Amer. Meteor*. Soc., **80,** 381–388.

Wakimoto, R. M., and V. N. Bringi, 1988: Dual-polarization observations of microbursts associated with intense convection: The 20 July storm during the MIST project. *Mon. Wea. Rev.,***116,** 1521–1539.

Whiton, R.C., P.L. Smith, S.G. Bigler, K.E. Wilk, and A.C. Harbuck, 1998: History of operational use of weather radar by U.S. Weather Services. Part II: Development of Operational Doppler Weather Radars. *Wea. Forecasting*, **13,** 244 – 252.

Zrnić, D. S., 1987: Three-body scattering produces precipitation signature of special diagnostic value. *Radio Sci*., **22,** 76–86.

Zrnić, D. S. and A. V. Ryzhkov, 1999: Polarimetry for weather surveillance radars. *Bull. Amer. Meteor. Soc.*, **80,** 389–406.